Applied Catalysis B: Environmental 219 (2017) 629–639

Contents lists available at ScienceDirect

Applied Catalysis B: Environmental

journal homepage: www.elsevier.com/locate/apcatb

3D polymer hydrogel for high-performance atomic iron-rich catalysts for oxygen reduction in acidic media

Zhi Qiao[a], Hanguang Zhang[a], Stavros Karakalos[b], Sooyeon Hwang[c], Jing Xue[a], Mengjie Chen[a], Dong Su[c], Gang Wu[a,*]

[a] Department of Chemical and Biological Engineering, University at Buffalo, The State University of New York, Buffalo, NY 14260, USA
[b] Department of Chemical Engineering, University of South Carolina, Columbia, SC 29208, USA
[c] Center for Functional Nanomaterials, Brookhaven National Laboratory, Upton, NY 11973, USA

ARTICLE INFO

Article history:
Received 28 March 2017
Received in revised form 19 June 2017
Accepted 1 August 2017
Available online 3 August 2017

Keywords:
Electrocatalysis
Polymer hydrogel
Single atomic iron sites
Oxygen reduction
Acidic media

ABSTRACT

Current platinum group metal (PGM)-free carbon nanocomposite catalysts for the oxygen reduction reaction (ORR) in acidic electrolyte often suffer from rapid degradation associated with carbon corrosion due to the use of large amount of amorphoous carbon black supports. Here, we developed a new concept of using freestanding 3D hydrogel to design support-free Fe-N-C catalysts. A 3D polyaniline (PANI)-based hydrogel was used for preparing a new type of single atomic iron site-rich catalyst, which has exhibited exceptionally enhanced activity and stability compared to conventional Fe-N-C catalysts supported on amorphous carbon blacks. The achieved performance metric on the hydrogel PANI-Fe catalysts is one of the best ever reported PGM-free catalysts, reaching a half-wave potential up to 0.83 V *vs.* RHE and only leaving 30 mV gap with Pt/C catalysts (60 $\mu gPt/cm^2$) in challenging acidic media. Remarkable ORR stability was accomplished as well on the same catalyst evidenced by using harsh potential cycling tests. The well dispersion of atomic iron into partially graphitized carbon, featured with dominance of micropores and porous network structures, is capable of accommodating increased number of active sites, strengthening local bonding among iron, nitrogen and carbon, and facilitating mass transfer. The 3D polymer hydrogel approach would be a new pathway to advance PGM-free catalysts.

1. Introduction

Proton exchange membrane fuel cell (PEMFC) is one of the most high efficiency and clean energy conversion devices by using H_2 to generate electricity without CO_2 or other emission. This is a desirable power source for electric vehicles, stationary, and portable applications. Oxygen reduction reaction (ORR), processing at the cathode of PEMFCs, is a vital reaction, nonetheless, which is kinetically sluggish and demands a large amount of Pt metal as the catalyst to achieve high activity and durability especially in challenging acid media. To widely implement PEMFC technology for various applications in a sustainable manner, the Pt-based catalysts must be replaced due to their prohibitive cost, limited supplies, and isolated distribution. Therefore, development of high-performance platinum group metal (PGM)-free catalysts in acidic media for PEMFCs has become an urgent topic in the field of electrocatalysis [1–5].

Among all explored PGM-free formulations in the last decade, the nitrogen and iron "co-doped" carbon nanocomposite catalysts (Fe-N-C) have been recognized as the most promising replacement of Pt, showing encouraging activity [6–9]. However, the remaining large activity gap between Pt and PGM-free catalysts still needs to be bridged. More importantly, their ORR stability in the highly oxidative and corrosive acidic media remains a grand challenge [10,11]. So far, all reported highly active Fe-N-C catalysts have been not able to provide sufficient performance durability yet for acidic Nafion®-based PEMFCs [2]. These catalysts often suffer from rapid degradation at high potentials or voltages (*e.g.*, >0.6 V) that are relevant for PEMFC to achieve high energy conversion efficiency (>70%). Therefore, the stability problems must be solved before PGM-free catalysts become viable for practical applications [12]. Generally, the catalyst degradation likely results from various factors. Among others, corrosion of carbon component in catalysts would lead to the reduction of active sites and loss of electrical contacts. In fact, carbon is the dominant component in the Fe-N-C catalyst (*e.g.*, larger than 90 wt.%). Most of previous Fe-N-C catalysts were prepared by using large amount of high-surface-area

* Corresponding author.
E-mail address: gangwu@buffalo.edu (G. Wu).

http://dx.doi.org/10.1016/j.apcatb.2017.08.008
0926-3373/

carbon balck supports (*e.g.* Ketjenblack or Black Pearl, 2000) to improve active site dispersion [13–15]. The addition of carbon black support was often found indispensible to achive high activity as determiend by using rotating disk electrode tests in aqueous electrolyte and Nafion® -based fuel cell tests [16,17]. However, carbon is not thermodynamically stable in the presence of water when electrode potentials are higher than its standard potential (0.21 V *vs.* SHE). Carbon tends to be oxidized in the harsh and oxidative ORR environment. Therefore, the amorphoous carbon blacks in catalysts have caused significnat carbon corrosion problems associated with catalyst degardation [15,18,19]. Also, the existence of extra inert carbon supports in catalysts also results in highly heterogeneous morphology and significant reduction of volume metric activity. To this end, development of effective synthetic chemistry to eliminate the use of amorphous carbon support is highly demanded to advance PGM-free carbon catalysts. Some template approaches have been exploring to remove the carbon black support during the catalyst synthesis including the use of TiO_2, MWNT, sacrificial supports, metal organic frameworks (MOF), and carbon gels [20–23]. Especially the support-free MOF approach, initially proposed by Liu at Argonne National Laboratory [24,25] and Dodelet at INRS [26,27], provided a new opportunity to prepare high-performance catalyst without using carbon supports.

Here, we reported an effective polymer hydrogel approach to preparing high-performance catalysts without using carbon black supports, which has demonstrated exceptionally enhanced activity and stability compared to current Fe-N-C catalysts. Hydrogel is a three-dimensional (3D) network containing large amount of water [28]. The hydrogel precursors would yield 3D porous catalyst architectures, potentially benefiting the improvements of active site density, mass/charge transfer, and structural integrity [29–31]. In this work, the polymer selected to prepare hydrogel is crosslinked polyaniline (PANI) that has been proved to be an effective nitrogen/carbon precursor [3]. PANI is rich in aromatic structures similar to graphitized carbon, which contains abundant carbon and nitrogen sources and easy to directly convert to graphitized carbon [3,32] During the hydrogel formation, inexpensive iron (III) chloride ($FeCl_3$) are used as co-oxidant to polymerize aniline as well as the iron doping source attached to functional groups of PANI. Therefore, the Fe-doped PANI hydrogel, consisting of iron, nitrogen, and carbon sources, was used as sole precursor to prepare Fe-N-C catalysts without adding extra amorphous carbon black supports. Subsequent thermal activation enables to convert the 3D polymer hydrogel into interconnecting carbon networks accommodating active sites associated with the doping of nitrogen and iron [33]. The effectiveness of PANI being precursors along with the unique 3D porous hydrogel framework were expected to provide great benefits to increase the number of active sites and enhance the robustness of carbon structure in catalysts. Furthermore, compared to single precursor, multiple nitrogen/carbon precursors provide great opportunity to tune catalyst morphology and microstructure favorable for ORR catalysis [34]. Thus, we added the secondary nitrogen/carbon compounds including ethylenediamine (EN) and melamine (MLMN) into PANI hydrogel to tune the N to C ratios in precursors as well as to increase complexing groups to enhance iron site dispersion. As a result, the binary PANI-EN hydrogel-derived catalyst demonstrated the best performance in both activity and stability. Compared to conventional PANI-Fe-C catalysts by physically mixing metal, nitrogen, and additional carbon back supports, the catalysts produced by polymer hydrogel have represented better reproducibility, more homogeneous morphology, and much enhanced catalyst activity and stability. Therefore, this hydrogel strategy provides a new pathway to advance PGM-free catalysts with more favorable morphology and structure for the ORR especially in more challenging acidic media.

2. Experimental section

2.1. Catalysts synthesis

In the typical procedures to prepare Fe-PANI-hydrogel catalyst, 0.33 g aniline (3.54 mmol) and 0.81 g ammonia persulfate (APS) (3.54 mmol) were dissolved in 2.0 M hydrogen chloride (HCl) solution (2.5 ml), respectively, to denote as solutions 1 and 2. Next, the solution 1 and 2 were incubated under 0 °C for 10 min. Then, the solution 2 (APS) was gradually added into the solution 1 containing aniline, and the polymerization reaction of aniline was conducted at 0 °C for about 10 min, following by adding 1.15 g iron chloride (7.1 mmol) at 0 °C for another 10 min reaction. Finally, the gel was aged at room temperature for at least 24 h before freeze-drying. The freeze-drying process is critical to retain the porous 3D structure of polymer hydrogel. The resulting gel-like solid (without any grinding) was immediately transferred into a tube furnace. The furnace temperature was increased gradually from room temperature to 900 °C with a ramping rate of 3 °C/min and held for 1 h under nitrogen gas (N_2) flow. The pyrolyzed solid was leached in 0.5 M H_2SO_4 at 80 °C for 5 h followed by a second heating treatment at 900 °C for 3 h under N_2 flow. As for binary PANI-MLMN-hydrogel and PANI-EN-hydrogel catalysts, the optimized molar ratios of PANI: MLMN and PANI: EN is 2.0. The given amount ethylenediamine and melamine were mixed with aniline in solution 1, respectively. The rest of the synthesis procedures is identical to the Fe-PANI-hydrogel catalyst.

2.2. Physical characterization

Brunauer-Emmett-Teller (BET) surface area was measured by using N_2 adsorption/desorption at 77 K on a Micromeritics TriStar II. Scanning electron microscopy (SEM) images were analyzed on a Hitachi SU 70 microscope at a working voltage of 5 kV. Transmission electron microscopy (TEM) was conducted on a JEOL 2100F and an aberration-corrected Hitachi 2700C scanning transmission electron microscope (STEM) at a voltage of 200 kV. X-ray diffraction (XRD) was analyzed by using a Rigaku Ultima IV diffractometer with Cu K-α X-rays. X-ray photoelectron spectroscopy (XPS) was performed with a Kratos AXIS Ultra DLD. X-ray photoelectron spectroscopy (XPS) equipped with a hemispherical energy analyzer and a monochromatic Al Kα source operated at 15 k eV and 150 W and pass energy was fixed at 40 eV for the high-resolution scans. All samples were prepared as pressed powders supported on a metal bar for XPS measurements. For this case, the FWHM of the major XPS peaks range from 0.3 eV to 1.7 eV for various elements. All the instrument parameters are constant including FWHMs, peak shapes, instrument design factors, chemical shifts, experimental settings and sample factors. The B.E. of Au was used as the reference. Raman spectra were collected on a Renishaw Raman system at 514 nm laser source. Samples were prepared as powders on a glass surface, with the excitation laser focused through a 100× microscope objective for a total interrogation spot size of ~1 μm diameter. Excitation power was held constant at ~150 μW for all samples. Scattered light was collected in backscatter configuration into an optical fiber, then dispersed through the Renishaw spectrometer and projected onto a CCD camera.

2.3. Electrochemical measurements

All electrochemical measurements were performed on a CHI Electrochemical Station (Model 760b) equipped with high-speed rotators. A rotating ring disk electrode (RRDE), which is from Pine Research Instrumental (model: AFE7R9GCPT, USA), was used as the working electrode. It contains glassy carbon disk and platinum ring: disk OD = 5.61 mm; ring OD = 7.92 mm; ID = 6.25 mm. A graphite rod with a diameter of 0.250 inch and a length of

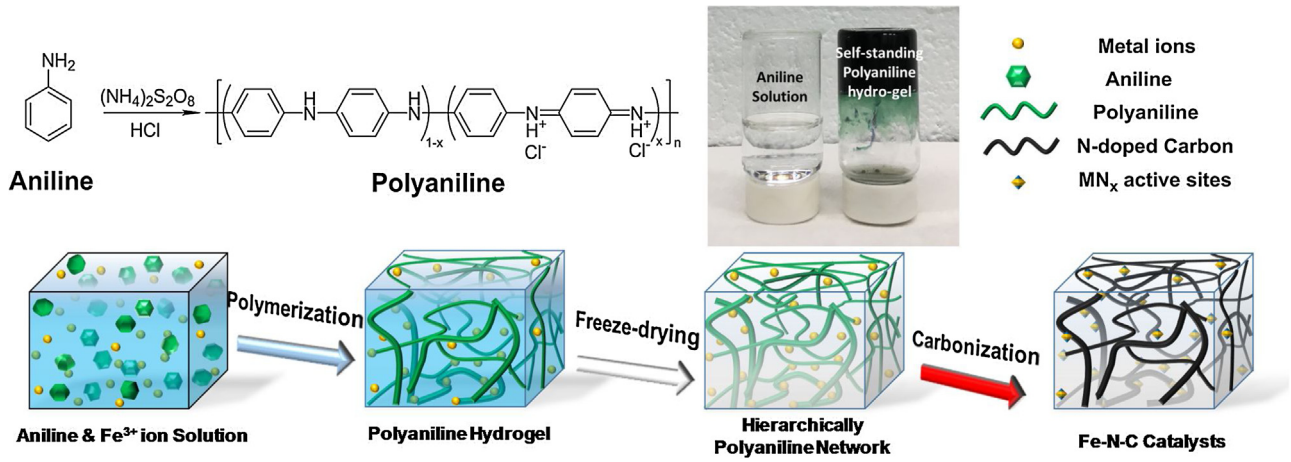

Fig. 1. Synthesis scheme of polyaniline hydrogel approach to prepare carbon support-free Fe-N-C catalysts.

12 inches and an $Hg/HgSO_4$ as the counter electrode and reference electrode, respectively. Catalyst powder (10 mg) and 5 wt% Nafion® solution (15 μl) were mixed with 1.0 ml isopropanol, and the resulting mixture was then sonicated vigorously for about 30 min to obtain a homogeneous ink. Afterwards, the ink was drop-casted onto the glassy carbon disk with 15-min-air drying at 60 °C. The loading of catalysts for all measurements was maintained at 0.6 mg/cm^2. All the cyclic voltammetry (CV) and ORR polarization curves were recorded in 0.5 M H_2SO_4. Electrochemical accessible surface areas were calculated by using double layer capacitance that was determined through CV at a scan rate of 20 mV/s in N_2 saturated 0.5 M H_2SO_4. The ORR activity was measured in 0.5 M H_2SO_4 saturated with O_2 at 900 rpm using steady-state polarization plots by holding each potential for 30 s with potential step of 30 mV. As ORR is a kinetically slow electrochemical reaction, the designed steady-state measurements is to allow the non-faradaic capacitance current passing through and accurately measure the cathodic current exclusively from the ORR. Hydrogen peroxide yield during the ORR was detected by using Pt ring electrode of RRDE that was applied a potential of 1.15 V *vs.* RHE. Durability of all catalysts was assessed in O_2 saturated 0.5 M H_2SO_4 solution by using two potential cycling windows ranging from 0.6 to 1.0 V and from 1.0 to 1.5 V at the same scanning rate of 50 mV/s, respectively. Especially, the high potential cycling mimics the carbon support stability protocol for Pt/C catalyst. Because there is no distinction between carbon and catalyst in PGM-free catalysts. This allow us to evaluate the carbon corrosion-related degradation of these catalysts during the start-up and shut-down of fuel cells.

3. Results and discussion

3.1. Catalyst synthesis through hydrogel approach

The polymer hydrogel approach to preparing Fe-N-C catalysts was illuminated in Fig. 1 by using PANI precursors. PANI is a polymer with relatively high mechanical flexibility, capable of offering 3D architecture to increase density of active sites. In addition to crosslinked PANI hydrogel, ethylenediamine (EN) and melamine (MLMN) as additional nitrogen/carbon precursors were chosen due to their unique molecular structures and effectiveness for being catalyst precursors [35–37]. MLMN, as a trimer of monomer cyanimide, containing high content of nitrogen by mass, has conjugated system of connected *p*-orbitals with delocalized electrons in molecules, which can easily generate nitrogen-doped carbon during heat treatment. Unlike MLMN, EN has a chain structure with two amine groups, which makes it easy to form not only copolymer with PANI, but also heterocycles during the formation of hydrogel. This feature may contribute to the generation of stable carbon structures, which is discussed later. In addition, all these precursors are inexpensive to achieve low-cost PGM-free Fe-N-C catalysts.

During the synthesis, starting with the iron doping into PANI-based hydrogels, freeze-drying process will directly transfer hydrogel into a 3D framework precursor with uniformly dispersed iron doping. Subsequent thermal treatment at the elevated temperature converts the framework into a porous carbon matrix with N and Fe doping. Furthermore, to eliminate undesired functional groups and unstable species, acid leaching treatment is crucial for generating active and stable catalysts. The second high-temperature treatment will further enhance and stabilize the catalyst by removing oxygen containing functional groups formed during acid leaching. Due to absence of the inert carbon black support, hydrogel-derived catalysts are able to provide an increased density of active sites and opening structures with high surface areas, which is favorable for ORR catalysis.

3.2. Catalytic activity and stability for the ORR

Due to the advantages of 3D polymer hydrogel precursors, three different Fe catalysts were prepared using various nitrogen/carbon precursors including individual PANI, and binary PANI-EN and PANI-MLMN. For the comparison, both carbon-black-free and ketjenblack (KJ) supported PANI-Fe catalyst were prepared through traditional methods as well [3]. Their catalytic activities and stabilities were systematically studied to evaluate the advantages of using polymer hydrogel precursors as well as the promotional role of adding the secondary nitrogen/carbon precursor such as melamine or ethylenediamine.

Fig. 2a gives a comprehensive comparison for different kinds of Fe catalysts prepared from traditional and the support-free hydrogel methods. The relevant catalytic performance metrics for various catalysts were also compared in Table S1. The traditional Fe-PANI catalyst without adding carbon support exhibited poor ORR activity with a much negative half-wave potential ($E_{1/2}$) around 0.68 V. However, the onset potential (E_{onset}) of the ORR is up to 0.90 V. The "onset potential" for the ORR was determined as the starting potential to generate measurable current density of 0.1 mA/cm^2. The poor $E_{1/2}$ suggests a significantly low density of active sites in the catalyst, which is in good agreement with a low surface area and aggregated morphology shown in Fig. S1. When using high surface area KJ black support to prepare Fe-PANI catalysts, the performance is improved significantly with a $E_{1/2}$ around 0.79 V, indication of the indispensable role of carbon support for tradi-

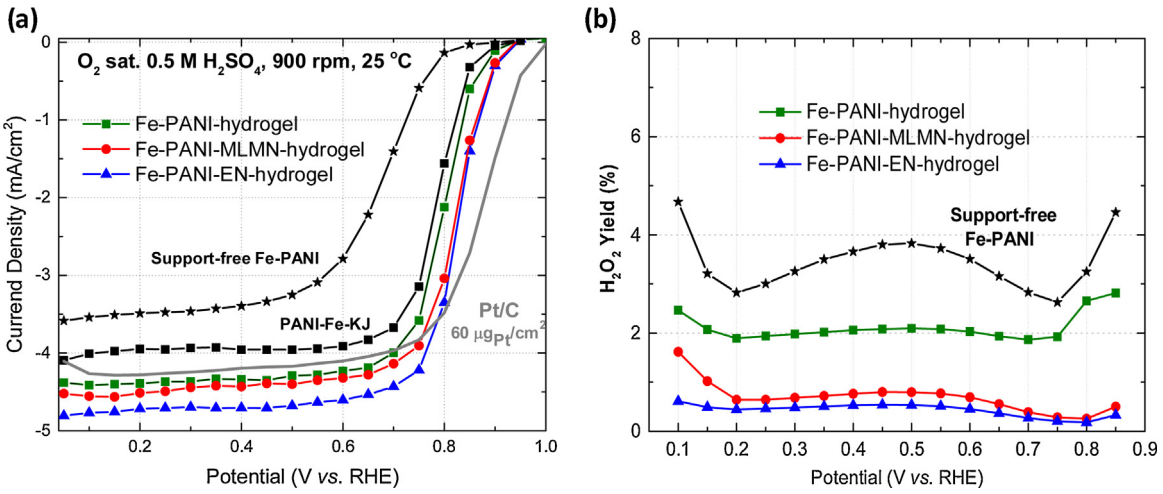

Fig. 2. (a) Steady-state ORR polarization plots of various Fe-N-C catalysts measured at 25 °C and 900 rpm in O_2 saturated 0.5 M H_2SO_4 (b). Four-electron selectivity is determined by using hydrogen peroxide yield during the ORR.

tional PANI-Fe catalysts. However, the hydrogel PANI-Fe precursor allows us to eliminate the use of carbon supports, and exhibited comparable or even improved performance showing E_{onset} and $E_{1/2}$ of 0.93 and 0.80 V, respectively. Furthermore, after adding the secondary nitrogen/carbon precursors, both Fe-PANI-EN and Fe-PANI-MLMN-hydrogel catalysts demonstrated even higher ORR activity with E_{onset} of 0.95 V and $E_{1/2}$ of 0.83 V. The newly achieved ORR activity in the challenging acidic media is one of the best Fe-N-C catalysts [38,39]. It clearly indicated that the addition of ethylenediamine or melamine into PANI hydrogel is effective to increase density of active sites as evidenced by more positive $E_{1/2}$. Importantly, the support-free hydrogel method enable to increase the density of active sites when compared to traditional ketjenblack supported PANI-Fe. The desired four-electron selectivity during the ORR was also determined using RRDE to measure the H_2O_2 yield. In good agreement with previously studied Fe-N-C catalysts, the overall H_2O_2 yield measured with three Fe catalysts is less than 2%. Especially, the Fe-PANI-EN-hydrogel and Fe-PANI-MLMN-hydrogel catalysts present a negligible H_2O_2 yield less than 1%. It is noted that the weak loading dependence of the peroxide yield at PANI-derived catalysts was observed relative to that observed with some other PGM-free catalysts that was demonstrated by Bonakdarpour et al. [40]. To determine kinetics of ORR on these various Fe-N-C catalysts, their Tafel plots were obtained based on the recorded polarization plots (Fig. S2). Their corresponding Tafel slopes are summarized in Table S2. All Fe-N-C catalysts exhibited similar Tafel slopes in the low overpotential range, suggesting their similar ORR reaction mechanisms. Based on kinetic analysis, a Tafel slope of 118 mV/dec suggests that the first electron transfer is the rate determining step, and a slope of 60 mV/dec likely involve a RDS with surface migration of intermediates. Thus, slopes between 70 and 90 mV/dec measured with these PANI-Fe catalysts indicate a mixed control from both charge transfer and intermediate migration.

Compared to activity improvement for PGM-free catalysts in acidic media, enhanced stability is more demanded for practical applications such as PEMFCs. So far, there is no any PGM-free catalyst that can demonstrate sufficient stability in acid at practical fuel cell operation voltages (>0.6 V). Therefore, stability of all studied Fe catalysts has been carefully evaluated to determine the possible promotional role stemming from hydrogel approach. We applied potential cycling stability tests, because they are more rigorous than measuring the decay in current density with time at a constant potential [41,42]. In addition to traditional (standard U.S. DOE protocol) accelerated stressing tests (AST) using potential cycling at relative low potential window (0.6–1.0 V), we also employed much more harsh AST conditions especially for carbon materials using cycling at a higher potential window (1.0–1.5 V) in O_2 saturated 0.5 M H_2SO_4 solution to study carbon corrosion in catalysts. During fuel cell operation, both the shut-off and start-on process lead to extremely high potential up to 1.5 V in cathode side due to H_2 starvation at anode. Therefore, cathode catalysts should be stable for a short period time at high potential. Following both AST protocols, cycling stability tests for three catalysts were carried out and compared in Fig. 3. Among others, the Fe-PANI-EN-hydrogel catalysts in acidic media exhibited the best stability during two ASTs at different potential windows. When the low potential cycling (0.6–1.0 V) was employed, there is only 14 mV loss in $E_{1/2}$ after 10,000 cycles (Fig. 3a). Under the identical testing conditions, Fe-PANI and Fe-PANI-MLMN hydrogel catalysts suffer from 29 and 22 mV loss, respectively. The Fe-N-C catalysts derived from traditional PANI shows significant loss (80 mV after 5000 cycles, Fig. S3a). The hydrogel approach yields much more stable catalysts, probably because of the elimination of amorphous carbon supports. Furthermore, under the more challenging high potential AST (1.0–1.5 V), the Fe-PANI-EN-hydrogel catalyst has a loss of 79 mV in $E_{1/2}$ after 10,000 cycles (Fig. 3b). Given such hash AST conditions for PGM-free catalysts up to 1.5 V, this loss is not unacceptable. The activity losses of the other two hydrogel-derived catalysts from PANI and PANI-MLMN precursors are up to 247 and 268 mV, respectively. Noteworthy, as no obvious shifts occur in E_{onset}, it can be speculated that the degradation of catalyst activity is mainly due to the decreased number of active sites associated with the reduction of active surface areas associated with carbon corrosion. Meanwhile, to provide insight into activity loss during the hash high potential cycling, we determined the changes of electrochemically accessible surface areas (EAS) of studied catalysts. As shown in Fig. S4, the ESAs reflected from capacitance was measured for Fe-PANI-hydrogel and Fe-PANI-EN-hydrogel catalysts before and after ASTs between 1.0 and 1.5 V. The Fe-PANI-Hydrogel catalyst present a significant ESA loss (nearly 80%), indicating corrosion of carbon phase in it. On the other hand, the Fe-PANI-EN-hydrogel catalyst shows reduced loss of ESA around 50%. This comparison represents that the carbon phases derived from PANI-EN has enhanced corrosion tolerance compared with those from individual PANI. Therefore, among studied catalysts, the hydrogel catalyst derived from PANI-EN binary precursors exhibited least catalyst degradation and carbon corrosion. As shown in Fig. S5, we also explored ternary PANI-MLMN-EN

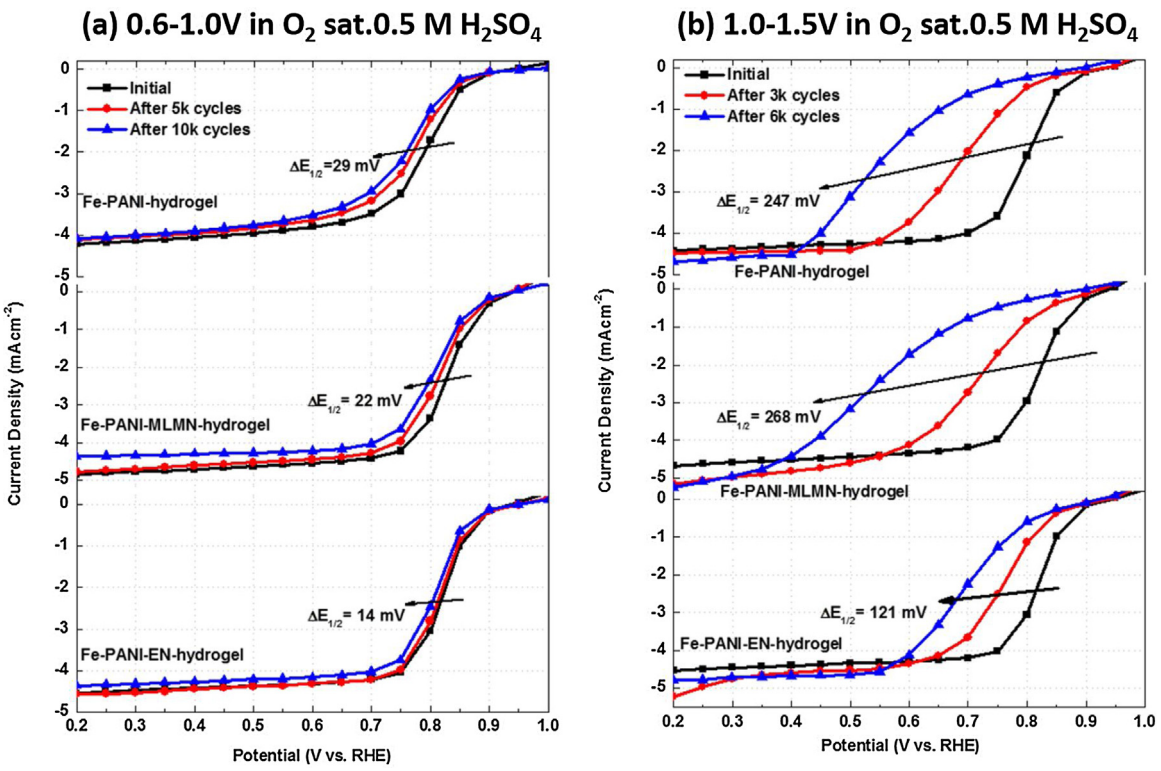

Fig. 3. Potential cyclic stability of the three catalysts between (a) 0.6–1.0 V vs RHE and (b) 1.0–1.5 V vs RHE at a scan rate of 50 mV/s in O_2 saturated 0.5 M H_2SO_4 electrolytes.

hydrogel-derived Fe catalysts, but not showing further improved activity and stability.

3.3. *Catalyst structure and morphology*

To elucidate the insight into the origin of enhancing catalyst activity and stability by adding EN into PANI hydrogel, we carefully compared catalysts' structures and morphologies. In general, during high temperature pyrolysis, the precise control of morphology and interaction among different component (N, C, and Fe) in the precursors is of vital importance for achieving high activity and stability [7]. Compared to oxide catalysts, one of the advantages of carbon-based catalysts is their porous structure and high surface area [43]. Thus, we investigated the role of specific surface area and pore size distribution played in influencing catalyst activity and durability when the hydrogel precursors were used for catalyst synthesis.

BET analysis was carried out by using N_2 physisorption at 77 K (Fig. 4). In principle, the high surface area microstructure presenting an ideal porosity is able to benefit overall ORR catalysis. All of these hydrogel-derived catalysts have relatively high specific surface area (more than 1200 m^2/g), which is much greater than state of the art Fe-N-C catalysts (600–900 m^2/g) [2,27,39]. The exceptionally increased surface areas indicate that hydrogel is an effective method to generate highly porous carbon matrix accommodating abundant active sites. Also, compared tothe Fe-PANI-hydrogel (1200 m^2/g) and Fe-PANI-MLMN-hydrogel (1306 m^2/g) catalysts, the Fe-PANI-EN-hydrogel catalyst processes the largest specific surface area up to 1400 m^2/g, which is likely contributable to the highest ORR activity measured with the catalyst. Regarding the pore size distribution (Fig. 4b and Table S3), the hierarchical porous network of the carbon framework is dominated by micropores (pore width <2.0 nm) in all three catalysts. Furthermore, it is obvious that the existing of MLMN or EN decrease the average size of micropores, and the Fe-PANI-EN-hydrogel catalyst is identified with the smallest micropores in the carbon framework. In general, micropores of the carbon framework are crucial for catalytic activity since they are related to accommodation of active sites [1,26,44]. Hence, this hydrogel synthesis method is favorable for forming micropore structure in carbon phases, thus facilitating the ORR catalysis [45]. Compared to others, smaller micropores (pore width < 0.8 nm) dominant in the Fe-PANI-EN catalysts should be responsible for the further enhanced activity (Fig. 4b).

To investigate the role of combination of binary nitrogen/carbon precursors played in controlling the overall carbon microstructure, corresponding microscopy analysis was carried out. SEM images showed in Fig. 5 provide a comprehensive comparison of three different hydrogel precursors and their corresponding catalysts. For the Fe-PANI-hydrogel catalyst, the well-defined porous long fiber-like PANI in precursor is converted into short rod-like inter-connected assembled structure in the catalyst after thermal activation and acidic treatment. It is able to retain porous network of 3D hydrogel showing a high BET surface area (1200 m^2/g). With addition of MLMN, the fiber diameter of PANI is reduced from 300 nm to 200 nm surrounding with small particles, which is believed contributed by MLMN. Unlike rod-like morphology observed with individual PANI hydrogel catalyst, the subsequent heating treatment generated highly porous nanosheet-like structures abundant in the PANI-MLMN-hydrogel catalyst. This is in good agreement with the increased BET surface area (1306 m^2/g) and total pores volume (0.66 cm^3/g) measured with the Fe-PANI-MLMN-hydrogel catalyst relative to Fe-PANI hydrogel catalyst. MLMN was found to be an effective precursor to generate nanosheet-like carbon structures after thermal conversion in the presence of iron sources, which is probably caused by its unique aromatic structures [37]. Likewise, the addition of EN into PANI hydrogel leads to a further reduced fiber diameter down to 150 nm in the precursor. After high-temperature treatment, the catalyst is dominant with 3D framework carbon network connected with nanofibers directly converted from PANI in precursors. The sub-

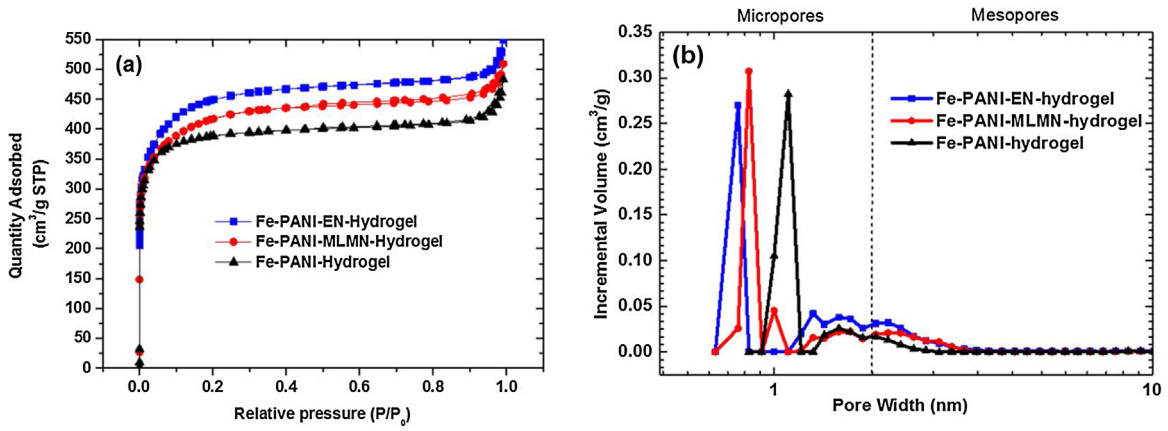

Fig. 4. BET surface areas (a), corresponding pore size distribution (b) for various Fe-N-C catalysts prepared through hydrogel approach.

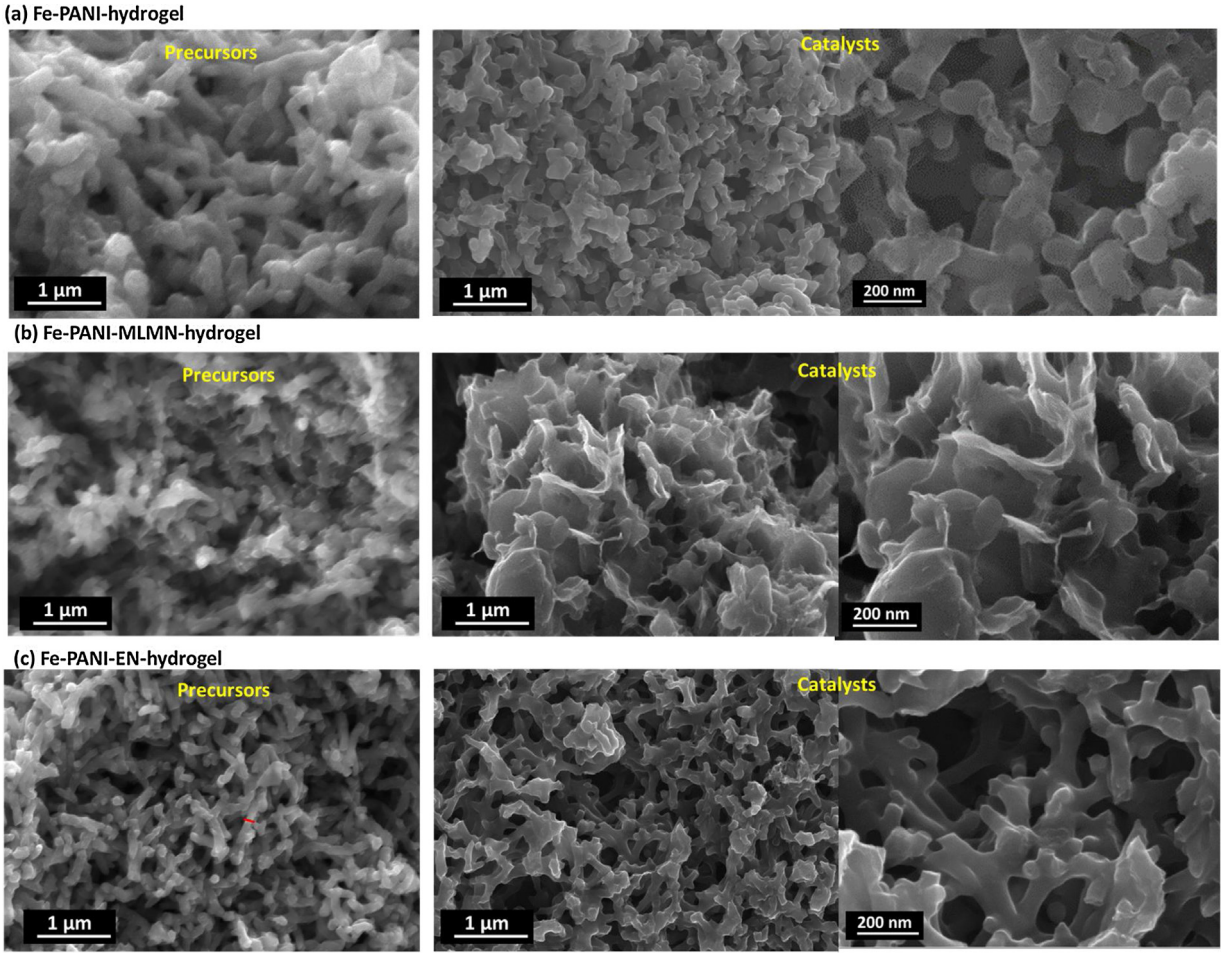

Fig. 5. SEM images for various hydrogel precursors and final catalysts for (a) PANI, (b) PANI-EN, and (c) PANI-MLMN.

stantial opening structure with dominant micropores yields the largest specific surface area (1400 m^2/g). To investigate carbon corrosion during stability tests, SEM images of three catalysts after harsh potential cycling (1.0–1.5 V) are also compared in Fig. S6. The degraded Fe-PANI catalyst presents more dense carbon structures with large particle sizes, in which the fiber-like carbon structures nearly disappear due to fusion process during carbon oxidation. The potential cycling also results in collapse of carbon phases in the Fe-PANI-MLMN catalyst. The original nanoshells and nanosheets are vanished, resulting in agglomerated carbon phases with more dense morphology. These significant changes of carbon structures are in good agreement of significant activity loss observed with the Fe-PANI and Fe-PANI-MLMN catalysts. Oppositely, the Fe-PANI-EN-hydrogel catalyst is able to maintain its highly porous morphology. Even more opening structures appear after the stability tests, probably due to the removal of less stable amorphous carbon phases. The robust 3D interconnected fiber carbon structure observed with Fe-PANI-EN-hydrogel catalyst demonstrated the exceptionally enhanced stability.

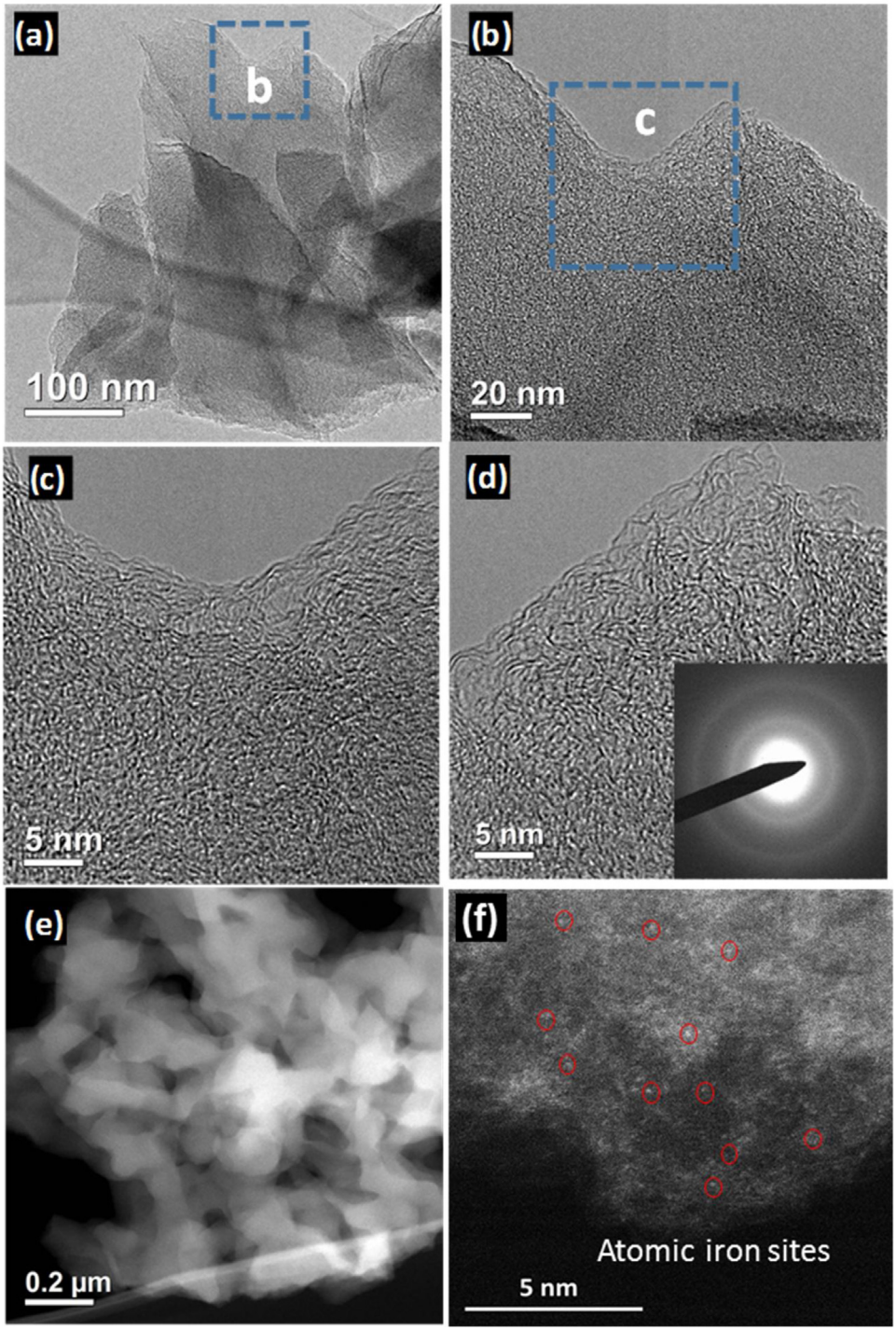

Fig. 6. TEM (a, b, c, and d) and STEM (e and f) images for the best performing Fe-PANI-EN-hydrogel catalysts. The inset of (d) is the selected electron diffraction pattern. (f) A high-resolution HAADF-STEM image showing Fe atoms.

Advanced STEM and HR-TEM images shown in Fig. 6 give more detailed information of the favorable microstructures of carbon phase for the best performing Fe-PANI-EN-hydrogel catalyst. In good agreement with SEM images, partially graphitized carbon structures is dominant in the catalyst (Fig. 6a). The curved carbon lattice fringes are abundant (Fig. 6b–d), which suggests the existence of disordered structures containing odd numbered five- and seven-membered carbon rings throughout the overall carbon phases. This highly disordered feature may contribute to the increase of active site density for the catalyst. Agreeing with XRD patterns, there is no any metallic iron aggregates appearing in the catalyst from both TEM (Fig. 6a) and STEM (Fig. 6e) imaging. Electron diffraction pattern shown in the inset of Fig. 6d further verified the absence of any crystalline phase in the catalyst. In a high-resolution (HR) high angle annular dark-field (HAADF)-STEM image in Fig. 6f and Fig. S7, single Fe atoms are observed. It should be noted that existence of iron in catalysts was clearly detected by using EELS (Fig. S7) and XPS. Therefore, as indicated by STEM, the form of iron in the catalyst is atomic single sites, which are

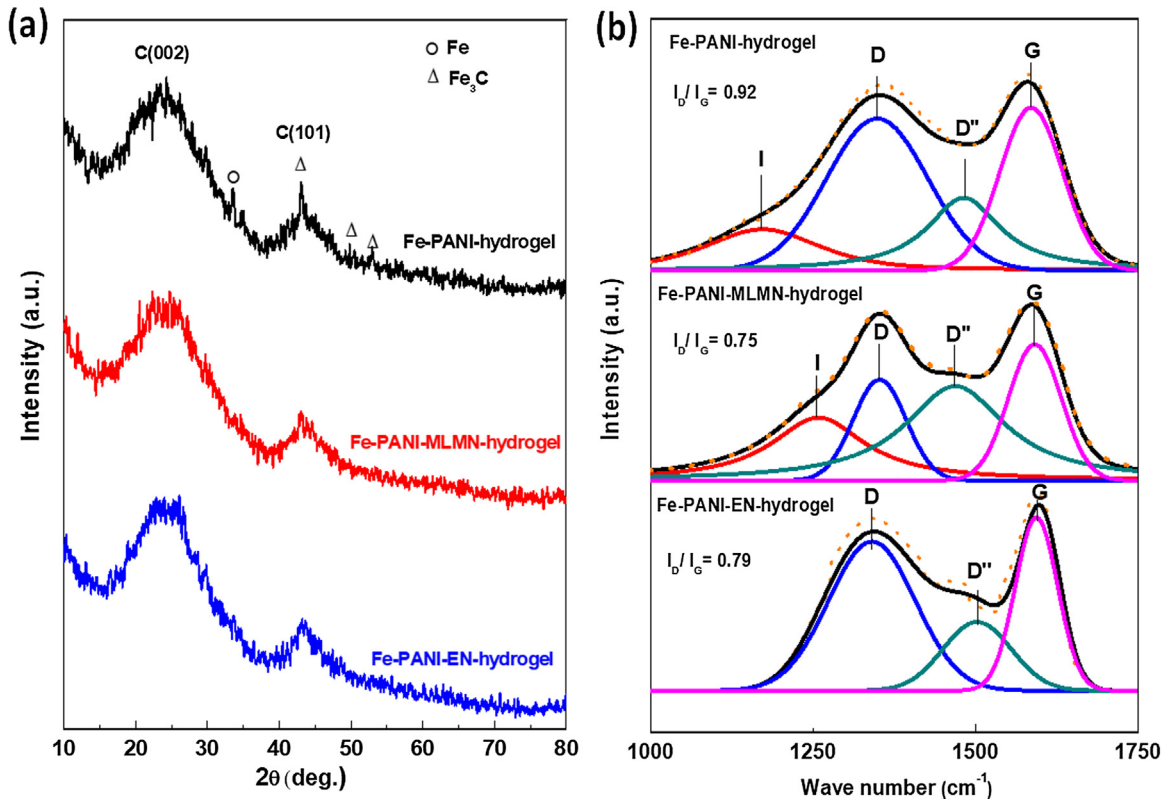

Fig. 7. (a) X-Ray diffraction patterns and Raman spectroscopy (b) of all three hydrogel-derived Fe-N-C catalysts.

likely bonded to nitrogen and carbon embedded into these partially graphitized carbon phases [46].

3.4. Graphitization degree, crystalline phases and nitrogen doping

To determine the crystalline phases and degree of graphitization of each catalyst, XRD and Raman spectroscopy analysis were conducted and the results are presented in Fig. 7. As shown in Fig. 7a, XRD patterns of all three catalysts present broad peaks at 25° and 44° corresponding to carbon (002) and (101) planes, indicating dominant amorphous carbon structures. The Fe-PANI-EN-hydrogel catalyst presented a relatively narrow peak of (002) compared to the others, suggesting higher degree of graphitization in carbon phases. In addition, among all catalysts, only Fe-PANI-hydrogel catalysts gave a small sharp peak at 44°, which is likely associated with metallic iron phases such as Fe or Fe_3C [47,48]. Currently, presence of Fe/Fe_3C phases in catalysts is still under discussion in terms of its influence on ORR activity [39,49]. Some research results indicated that presence of Fe/Fe_3C has promotional role in enhancing ORR activity due to the possible capability to change electronic structures of carbon layers covering on them [50,51]. Here, the Fe/Fe_3C containing Fe-PANI-hydrogel catalysts have relatively lower catalytic activity and stability, suggesting that the Fe/Fe_3C phases have no benefits to ORR performance improvement for Fe-N-C catalysts synthesized from the hydrogel method.

As Raman spectroscopy shown in Fig. 7b, there are two prominent first order peaks corresponding to D and G for all three catalysts, indicating the formation of graphitic materials with various dislocation/defects. Furthermore, the peak intensity ratio ($I_{(D)}/I_{(G)}$) of the D (~1350 cm^{-1}) and G (~1590 cm^{-1}) bands was chosen to study degree of graphitization in carbon [16]. Lower value of $I_{(D)}/I_{(G)}$ indicates a higher degree of graphitization. Because of the very broad peaks of the D and G bands in three catalysts, peak fitting was performed following the procedure outlined in previous work [16,30,52]. The fitting results were summarized in Table S4. Both Fe-PANI-EN-hydrogel and Fe-PANI-MLMN-dyrogel exhibits the higher degree of graphitization due to its lowest value of $I_{(D)}/I_{(G)}$. This would benefit for improved catalytic stability during both ASTs. In addition to D and G bands, the I band appeared at a wide range (~1180–1290 cm^{-1}) and the D" band (~1500 cm^{-1}) are related to the disorder in the graphitic lattice [53–55]. Fe-PANI-hydrogel and Fe-PANI-MLMN-hydrogel catalysts have shown the clear I band and D" bands. However, there is no I band for Fe-PANI-EN-hydrogel catalyst, indicating relatively low disorder degree in the graphitic lattice. More dominant D" band with stronger intensity observed with both Fe-PANI-MLMN-hydrogel and Fe-PANI-EN-hydrogel catalyst indicates that the existing of MLMN or EN is able to increases the local disordered structures of carbon. Noteworthy, the MLME and EN catalysts have overall higher graphitization degree as evidenced by carbon (002) XRD peak along with the smaller ratio of $I_{(D)}/I_{(G)}$. Such structure is likely associated with the existence of porphyrin-like FeN_4C_{12} moieties in Fe-N-C catalysts, which demonstrated to form disordered graphitized carbon sheets by Andrea [38]. The unique feature, which combines disordered local structures and high graphitization degree in overall carbon phases, makes the Fe-PANI-EN-hydrogel catalyst process favorable carbon morphology for the greater activity and durability [34,56].

Nitrogen doping and local carbon bonding structures are believed to be crucial for overall catalytic performance in Fe-N-C catalysts. Based on this knowledge, the surface concentration of dopants for all the catalysts were analyzed by using XPS. Their corresponding N1s, C1s, and Fe 2p spectra are represented in Fig. 8. The relevant fitting results for high-resolution N1s and C1s peaks were summarized in Tables S5 and S6. In general, four types of doped N atoms were observed in these catalysts, including pyridinic-N (398.4 eV) at edge of carbon planes, a possible Fe-N bond at 399.4 eV, graphitic-N doped at interior carbon plane (401.0 eV), and oxidized pyridinic-N (404.8 eV) attached with oxygen. The absence

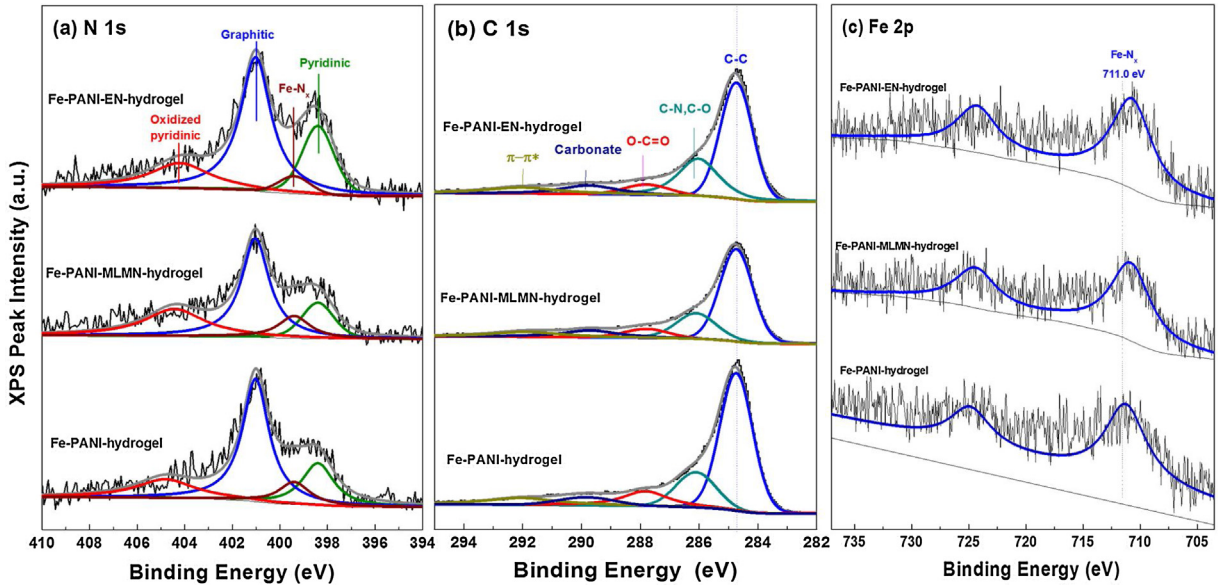

Fig. 8. High-resolution XPS (a) N1s, (b) C1s, and (c) Fe 2p spectra of all three hydrogel-derived Fe-N-C catalysts.

of pyrrolic N related to five side ring is due to its instability at the elevated temperature (>800 °C), which is in good agreement with previous observations [30,57,58]. As for pyridinc-N, its content measured with the Fe-PANI-EN-hydrogel catalyst is significantly higher than others, showing in line with the most positive $E_{1/2}$ potential meaning higher number of available active sties in the catalyst. This can also be verified by recent theoretical and experimental results showing that pyridinic N is directly associated with the active sites for the ORR [59,60]. High-resolution XPS C 1s peak revealed five different components presenting owing to the presence of various carbon moieties and π-π* interactions in the graphitic structure. Among studied catalysts, Fe-PANI-EN-hydrogel catalysts presented a relatively narrow peak for C—C, suggesting a higher degree of graphitization, which is in agreement with the XRD and Raman results. O 1s spectra shown in Fig. S8 indicated the Fe-PANI-EN-hydrogel catalyst contain less O—C=O content suggesting less amorphous structures. There are trace amount of sulfur detected in these catalysts, which is stemmed from the sulfur-containing APS used for polymerizing aniline during the formation of PANI hydrogel (Fig. S9). The peak at 164.4 eV and 168.4 eV can be attributed to $S_{2p3/2}$ of thiophene and SO_4^{2-}, respectively. The thiophene-like sulfur could behave similar to doped nitrogen as "one-e$^-$-donor" or "two-e$^-$-donor", thus facilitating the possible interaction with metals and carbon planes, respectively [61,62]. The elemental qualifications determined by using XPS for these three catalysts are shown in Table S7. Relative to Fe-PANI hydrogel, adding MLMN or EN has led to higher contents of both N and Fe. Although the absolute incremental is not significant, the trend of simultaneous increases of N and Fe resulting from the addition of EN is clear because the detectable limitation of XPS in this work is around 0.1 at.%. On the other hand, the Fe-PANI-hydrogel catalyst contains relatively less Fe content, although there were Fe or Fe_3C verified by the XRD analysis. This means that the tendency of iron forming atomic dispersion coordinating with N, rather than aggregates is greatly dependent on nitrogen/carbon precursors and resulting carbon structures. The additional carbon/nitrogen precursors integrated with PANI hydrogel is able to boost activity by generating more active sites. Fe 2p spectra (Fig. 8c) for these hydrogel derived catalysts exhibited a dominant peak at 711.0 eV. Wan et al., studied a material that includes Fe atoms connected with four nitrogen atoms. They attributed the Fe-N_4 complex to a peak at ~711 eV in the Fe 2p region and to a peak at 399.4 eV in the N 1s region [63,64]. In this work, both Fe 2p (711 eV) and N 1s (399.4 eV) peaks suggest the existence of Fe-N_4 coordination in the hydrogel-derived Fe-N-C catalysts is very likely. Meanwhile, there is no obvious peak at 707.0 eV and 720.2 eV indicating that there is nearly no metallic Fe, iron carbide, and iron oxide in surface layers of catalysts. Due to the low Fe content, the spectra associated with Fe is disturbing. However, among studied catalysts the peak intensity observed with the Fe-PANI-EN-hydrogel is the most dominant, suggesting the highest density of Fe-N_x active sites. Thus, the simultaneous increase of Fe and N contents observed with the binary precursor-derived catalysts showing enhanced activity is supportive to our speculation that increased number of active sites is associated with the formation of FeN_x sites. The partially graphitized carbon in Fe-PANI-EN-hydrogel catalysts seems to be favorable carbon phase for the ORR, which is able to accommodate large number of active sites with a possible formulation of FeN_xC_y [65].

4. Conclusions

In this work, a new approach to preparing highly active and stable Fe-N-C catalysts for the ORR in challenging acidic media was developed through using freestanding 3D crosslinked polyaniline hydrogel. Unlike conventional methods by using substantial inert and amorphous carbon black as a support, the PANI hydrogel preparation eliminates the use of support and yields enhanced activity and stability. This is due to that it can avoid serious carbon corrosion resulting from carbon black supports and significantly increase volumetric activity. Furthermore, adding secondary carbon/nitrogen precursors including ethylenediamine or melamine generates more favorable catalyst structures and morphologies capable of increasing density of active sites and improving stability. Instead of forming metallic aggregates such as Fe/FeC_3, dominant atomic single Fe sites are well dispersed into porous carbon, likely coordinating with pyridinic N as active sites (*e.g.*, FeN_x) for the ORR. In particular, the most active binary hydrogel-derived Fe-PANI-EN catalyst exhibited high ORR activity ($E_{1/2}$ = 0.83 V *vs.* RHE), only 30 mV gap remaining to that of Pt/C catalyst (60 $\mu g_{Pt}/cm^2$) in acids. Impressively improved durability in acidic media for the ORR was also achieved on the same catalyst, especially during potential cycling in both (0.6–1.0 V) and (1.0–1.5 V *vs.* RHE) windows. As a result, a new type of iron catalyst consisting of atomic iron-rich

sites embedded into porous carbon featured with disordered local structures (HR-TEM images) and overall high graphitization degree (Raman analysis) were prepared, which demonstrated remarkably improved activity and stability in challenging acidic electrolytes.

Overall, we demonstrated that use of polymer hydrogel precursors is an effective approach to producing a high-performance atomic iron catalyst. When compared to current Fe-N-C catalysts by mixing metal, nitrogen, and additional carbon black supports together, the 3D polymer hydrogel approach can provide homogeneous morphology with better reproducibility during the synthesis as well as exceptionally improved activity and stability. This approach would provide a new pathway to develop advanced PGM-free catalysts with much improved ORR performance for acidic PEMFCs.

Acknowledgements

The authors acknowledge financial support for the start-up funding from the University at Buffalo (SUNY) along with National Science Foundation (CBET-1604392) and U.S. Department of Energy, EERE, Fuel Cell Technologies Office (FCTO). TEM and STEM analysis were performed at the Center for Functional Nanomaterials, a U.S. DOE Office of Science Facility, at Brookhaven National Laboratory under Contract No. DE-SC0012704.

Appendix A. Supplementary data

Supplementary data associated with this article can be found, in the online version, at http://dx.doi.org/10.1016/j.apcatb.2017.08.008.

References

[1] M. Lefèvre, E. Proietti, F. Jaouen, J.-P. Dodelet, Iron-based catalysts with improved oxygen reduction activity in polymer electrolyte fuel cells, Science 324 (2009) 71–74.
[2] G. Wu, A. Santandreu, W. Kellogg, S. Gupta, O. Ogoke, H. Zhang, H.-L. Wang, L. Dai, Carbon nanocomposite catalysts for oxygen reduction and evolution reactions: from nitrogen doping to transition-metal addition, Nano Energy 29 (2016) 83–110.
[3] G. Wu, K.L. More, C.M. Johnston, P. Zelenay, High-performance electrocatalysts for oxygen reduction derived from polyaniline, iron, and cobalt, Science 332 (2011) 443–447.
[4] M. Luo, Y. Sun, L. Wang, S. Guo, Tuning multimetallic ordered intermetallic nanocrystals for efficient energy electrocatalysis, Adv. Energy Mater. 7 (2016), 1602073, http://dx.doi.org/10.1002/aenm.201602073.
[5] Q. Wu, L. Yang, X. Wang, Z. Hu, From carbon-based nanotubes to nanocages for advanced energy conversion and storage, Acc. Chem. Res. 50 (2017) 435–444.
[6] J. Zhang, L. Dai, Heteroatom-doped graphitic carbon catalysts for efficient electrocatalysis of oxygen reduction reaction, ACS Catal. 5 (2015) 7244–7253.
[7] G. Wu, P. Zelenay, Nanostructured non-precious metal catalysts for oxygen reduction reaction, Acc. Chem. Res. 46 (2013) 1878–1889.
[8] Q. Jia, N. Ramaswamy, H. Hafiz, U. Tylus, K. Strickland, G. Wu, B. Barbiellini, A. Bansil, E.F. Holby, P. Zelenay, Experimental observation of redox-induced Fe-N switching behavior as a determinant role for oxygen reduction activity, ACS Nano 9 (2015) 12496–12505.
[9] M.J. Workman, A. Serov, L.-k. Tsui, P. Atanassov, K. Artyushkova, Fe-N-C catalyst graphitic layer structure and fuel cell performance, ACS Energy Letters (2017) 1489–1493.
[10] G. Wu, K. Artyushkova, M. Ferrandon, A.J. Kropf, D. Myers, P. Zelenay, Performance durability of polyaniline-derived non-precious cathode catalysts, ECS Trans. 25 (2009) 1299–1311.
[11] M. Ferrandona, X. Wang, A.J. Kropfa, D.J. Myersa, G. Wu, C.M. Johnston, P. Zelenay, Stability of iron species in heat-treated polyaniline-iron-carbon polymer electrolyte fuel cell cathode catalysts, Electrochim. Acta 110 (2013) 282–291.
[12] G. Zhang, R. Chenitz, M. Lefèvre, S. Sun, J.-P. Dodelet, Is iron involved in the lack of stability of Fe/N/C electrocatalysts used to reduce oxygen at the cathode of PEM fuel cells? Nano Energy 29 (2016) 111–125.
[13] F. Jaouen, E. Proietti, M. Lefèvre, R. Chenitz, J.-P. Dodelet, G. Wu, H.T. Chung, C.M. Johnston, P. Zelenay, Recent advances in non-precious metal catalysis for oxygen-reduction reaction in polymer electrolyte fuel cells, Energy Environ. Sci. 4 (2011) 114–130.
[14] H. Sheng, M. Wei, A. D'Aloia, G. Wu, Heteroatom polymer-derived 3D high-surface-area and mesoporous graphene sheet-like carbon for supercapacitors, ACS Appl. Mater. Interfaces 8 (2016) 30212–30224.
[15] G. Wu, M.A. Nelson, N.H. Mack, S. Ma, P. Sekhar, F.H. Garzon, P. Zelenay, Titanium dioxide-supported non-precious metal oxygen reduction electrocatalyst, Chem. Commun. 46 (2010) 7489–7491.
[16] G. Wu, C.M. Johnston, N.H. Mack, K. Artyushkova, M. Ferrandon, M. Nelson, J.S. Lezama-Pacheco, S.D. Conradson, K.L. More, D.J. Myers, Synthesis–structure–performance correlation for polyaniline–Me–C non-precious metal cathode catalysts for oxygen reduction in fuel cells, J. Mater. Chem. 21 (2011) 11392–11405.
[17] Q. Li, G. Wu, D.A. Cullen, K.L. More, N.H. Mack, H. Chung, P. Zelenay, Phosphate-tolerant oxygen reduction catalysts, ACS Catal. 4 (2014) 3193–3200.
[18] G. Wu, K.L. More, P. Xu, H.-L. Wang, M. Ferrandon, A.J. Kropf, D.J. Myers, S. Ma, P. Zelenay, Carbon-nanotube-supported graphene-rich non-precious metal oxygen reduction catalyst with enhanced performance durability, Chem. Commun. 49 (2013) 3291–3293.
[19] W. Gao, D. Havas, S. Gupta, Q. Pan, N. He, H. Zhang, H.-L. Wang, G. Wu, Is reduced graphene oxide favorable for nonprecious metal oxygen-reduction catalysts? Carbon 102 (2016) 346–356.
[20] A. Serov, M.H. Robson, M. Smolnik, P. Atanassov, Tri-metallic transition metal–nitrogen–carbon catalysts derived by sacrificial support method synthesis, Electrochim. Acta 109 (2013) 433–439.
[21] W. Xia, J. Zhu, W. Guo, L. An, D. Xia, R. Zou, Well-defined carbon polyhedrons prepared from nano metal–organic frameworks for oxygen reduction, J. Mater. Chem. A 2 (2014) 11606–11613.
[22] W. Kiciński, B. Dembinska, M. Norek, B. Budner, M. Polański, P.J. Kulesza, S. Dyjak, Heterogeneous iron-containing carbon gels as catalysts for oxygen electroreduction: multifunctional role of sulfur in the formation of efficient systems, Carbon 116 (2017) 655–669.
[23] Z. Li, M. Shao, L. Zhou, R. Zhang, C. Zhang, M. Wei, D.G. Evans, X. Duan, Directed growth of metal-organic frameworks and their derived carbon-based network for efficient electrocatalytic oxygen reduction, Adv. Mater. 28 (2016) 2337–2344.
[24] H. Wang, F.-X. Yin, B.-H. Chen, X.-B. He, P.-L. Lv, C.-Y. Ye, D.-J. Liu, ZIF-67 incorporated with carbon derived from pomelo peels: a highly efficient bifunctional catalyst for oxygen reduction/evolution reactions, Appl. Catal. B: Environ. 205 (2017) 55–67.
[25] H.M. Barkholtz, D.-J. Liu, Advancements in rationally designed PGM-free fuel cell catalysts derived from metal–organic frameworks, Mater. Horiz. 4 (2017) 20–37.
[26] E. Proietti, F. Jaouen, M. Lefèvre, N. Larouche, J. Tian, J. Herranz, J.-P. Dodelet, Iron-based cathode catalyst with enhanced power density in polymer electrolyte membrane fuel cells, Nat. Commun. 2 (2011) 416.
[27] M. Shao, Q. Chang, J.-P. Dodelet, R. Chenitz, Recent advances in electrocatalysts for oxygen reduction reaction, Chem. Rev. 116 (2016) 3594–3657.
[28] H. Guo, W. He, Y. Lu, X. Zhang, Self-crosslinked polyaniline hydrogel electrodes for electrochemical energy storage, Carbon 92 (2015) 133–141.
[29] C. Zhu, S. Fu, J. Song, Q. Shi, D. Su, M.H. Engelhard, X. Li, D. Xiao, D. Li, L. Estevez, D. Du, Y. Lin, Self-assembled fe–N-doped carbon nanotube aerogels with single-atom catalyst feature as high-efficiency oxygen reduction electrocatalysts, Small 13 (2017), 1603407, http://dx.doi.org/10.1002/smll.201603407.
[30] Z.-S. Wu, S. Yang, Y. Sun, K. Parvez, X. Feng, K. Müllen, 3D nitrogen-doped graphene aerogel-supported Fe_3O_4 nanoparticles as efficient electrocatalysts for the oxygen reduction reaction, J. Am. Chem. Soc. 134 (2012) 9082–9085.
[31] B. You, P. Yin, J. Zhang, D. He, G. Chen, F. Kang, H. Wang, Z. Deng, Y. Li, Hydrogel-derived non-precious electrocatalysts for efficient oxygen reduction, Sci. Rep. 5 (2015) 11739.
[32] N.-H. Xie, X.-H. Yan, B.-Q. Xu, Is ammonium peroxydisulfate indispensable for preparation of aniline-derived iron–nitrogen–carbon electrocatalysts? ChemSusChem 9 (2016) 2301–2306.
[33] Q. Jia, N. Ramaswamy, U. Tylus, K. Strickland, J. Li, A. Serov, K. Artyushkova, P. Atanassov, J. Anibal, C. Gumeci, S.C. Barton, M.-T. Sougrati, F. Jaouen, B. Halevi, S. Mukerjee, Spectroscopic insights into the nature of active sites in iron–nitrogen–carbon electrocatalysts for oxygen reduction in acid, Nano Energy 29 (2016) 65–82.
[34] S. Gupta, S. Zhao, O. Ogoke, Y. Lin, H. Xu, G. Wu, Engineering favorable morphology and structure of Fe-N-C oxygen-reduction catalysts via tuning nitrogen/carbon precursors, ChemSusChem 10 (2017) 774–785.
[35] V. Nallathambi, J.-W. Lee, S.P. Kumaraguru, G. Wu, B.N. Popov, Development of high performance carbon composite catalyst for oxygen reduction reaction in PEM proton exchange membrane fuel cells, J. Power Sources 183 (2008) 34–42.
[36] G. Wu, M. Nelson, S. Ma, H. Meng, G. Cui, P.K. Shen, Synthesis of nitrogen-doped onion-like carbon and its use in carbon-based CoFe binary non-precious-metal catalysts for oxygen-reduction, Carbon 49 (2011) 3972–3982.
[37] Q. Li, T. Wang, D. Havas, H. Zhang, P. Xu, J. Han, J. Cho, G. Wu, High-performance direct methanol fuel cells with precious-metal-free cathode, Adv. Sci. 3 (2016) 1600140.
[38] A. Zitolo, V. Goellner, V. Armel, M.-T. Sougrati, T. Mineva, L. Stievano, E. Fonda, F. Jaouen, Identification of catalytic sites for oxygen reduction in iron-and nitrogen-doped graphene materials, Nat. Mater. 14 (2015) 937–942.
[39] J.P. Dodelet, R. Chenitz, L. Yang, M. Lefèvre, A new catalytic site for the electroreduction of oxygen? ChemCatChem 6 (2014) 1866–1867.
[40] A. Bonakdarpour, M. Lefevre, R. Yang, F. Jaouen, T. Dahn, J.-P. Dodelet, J. Dahn, Impact of loading in RRDE experiments on Fe-N-C catalysts: two-or

four-electron oxygen reduction? Electrochem. Solid State Lett. 11 (2008) B105–B108.
[41] S. Zhang, X. Yuan, H. Wang, W. Mérida, H. Zhu, J. Shen, S. Wu, J. Zhang, A review of accelerated stress tests of MEA durability in PEM fuel cells, Int. J. Hydrogen Energy 34 (2009) 388–404.
[42] J. Wu, X.Z. Yuan, J.J. Martin, H. Wang, J. Zhang, J. Shen, S. Wu, W. Merida, A review of PEM fuel cell durability: degradation mechanisms and mitigation strategies, J. Power Sources 184 (2008) 104–119.
[43] H. Osgood, S.V. Devaguptapu, H. Xu, J.P. Cho, G. Wu, Transition metal (Fe, Co, Ni, and Mn) oxides for oxygen reduction and evolution bifunctional catalysts in alkaline media, Nano Today 11 (2016) 601–625.
[44] F. Jaouen, M. Lefèvre, J.-P. Dodelet, M. Cai, Heat-treated Fe/N/C catalysts for O_2 electroreduction: are active sites hosted in micropores? J. Phys. Chem. B 110 (2006) 5553–5558.
[45] M. Lefèvre, J.-P. Dodelet, Recent advances in non-precious metal electrocatalysts for oxygen reduction in PEM fuel cells, ECS Trans. 45 (2012) 35–44.
[46] U.I. Kramm, I. Herrmann-Geppert, J. Behrends, K. Lips, S. Fiechter, P. Bogdanoff, On an easy way to prepare metal–nitrogen doped carbon with exclusive presence of MeN_4-type sites active for the ORR, J. Am. Chem. Soc. 138 (2016) 635–640.
[47] V. Ordomsky, B. Legras, K. Cheng, S. Paul, A. Khodakov, The role of carbon atoms of supported iron carbides in Fischer–Tropsch synthesis, Catal. Sci. Technol. 5 (2015) 1433–1437.
[48] Q. Li, H. Pan, D. Higgins, R. Cao, G. Zhang, H. Lv, K. Wu, J. Cho, G. Wu, Metal-organic framework derived bamboo-like nitrogen-doped graphene tubes as an active matrix for hybrid oxygen-reduction electrocatalysts, Small 11 (2015) 1443–1452.
[49] K. Strickland, E. Miner, Q. Jia, U. Tylus, N. Ramaswamy, W. Liang, M.-T. Sougrati, F. Jaouen, S. Mukerjee, Highly active oxygen reduction non-platinum group metal electrocatalyst without direct metal-nitrogen coordination, Nat. Commun. 6 (2015) 7343.
[50] J.-S. Li, S.-L. Li, Y.-J. Tang, M. Han, Z.-H. Dai, J.-C. Bao, Y.-Q. Lan, Nitrogen-doped Fe/Fe_3C@ graphitic layer/carbon nanotube hybrids derived from MOFs: efficient bifunctional electrocatalysts for ORR and OER, Chem. Commun. 51 (2015) 2710–2713.
[51] Y. Hou, T. Huang, Z. Wen, S. Mao, S. Cui, J. Chen, Metal- organic framework-derived nitrogen-doped core-shell-structured porous Fe/Fe3C@ C nanoboxes supported on graphene sheets for efficient oxygen reduction reactions, Adv. Energy Mater. 4 (2014) 1400337.
[52] J.-M. Vallerot, X. Bourrat, A. Mouchon, G. Chollon, Quantitative structural and textural assessment of laminar pyrocarbons through Raman spectroscopy, electron diffraction and few other techniques, Carbon 44 (2006) 1833–1844.
[53] W. Bacsa, J. Lannin, D. Pappas, J. Cuomo, Raman scattering of laser-deposited amorphous carbon, Phys. Rev. B 47 (1993) 10931.
[54] N. McEvoy, N. Peltekis, S. Kumar, E. Rezvani, H. Nolan, G.P. Keeley, W.J. Blau, G.S. Duesberg, Synthesis and analysis of thin conducting pyrolytic carbon films, Carbon 50 (2012) 1216–1226.
[55] T. Jawhari, A. Roid, J. Casado, Raman spectroscopic characterization of some commercially available carbon black materials, Carbon 33 (1995) 1561–1565.
[56] H. Zhang, H. Osgood, X. Xie, Y. Shao, G. Wu, Engineering nanostructures of PGM-free oxygen-reduction catalysts using metal-organic frameworks, Nano Energy 31 (2017) 331–350.
[57] S. Gupta, L. Qiao, S. Zhao, Y. Lin, D.S. Vamsi, H. Xu, X. Wang, M. Swihart, G. Wu, Highly active and stable graphene tubes decorated with FeCoNi alloy nanoparticles via a template-free graphitization for bifunctional oxygen reduction and evolution, Adv. Energy Mater. 6 (2016) 1601198.
[58] Q. Li, P. Xu, W. Gao, S. Ma, G. Zhang, R. Cao, J. Cho, H.-L. Wang, G. Wu, Graphene/graphene tube nanocomposites templated from cage-containing metal-organic frameworks for oxygen reduction in Li-O_2 batteries, Adv. Mater. 26 (2014) 1378–1386.
[59] D. Guo, R. Shibuya, C. Akiba, S. Saji, T. Kondo, J. Nakamura, Active sites of nitrogen-doped carbon materials for oxygen reduction reaction clarified using model catalysts, Science 351 (2016) 361–365.
[60] J. Shui, M. Wang, F. Du, L. Dai, N-doped carbon nanomaterials are durable catalysts for oxygen reduction reaction in acidic fuel cells, Sci. Adv. 1 (2015) e1400129.
[61] G. Faubert, R. Côté, J. Dodelet, M. Lefevre, P. Bertrand, Oxygen reduction catalysts for polymer electrolyte fuel cells from the pyrolysis of FeII acetate adsorbed on 3 4, 9, 10-perylenetetracarboxylic dianhydride, Electrochim. Acta 44 (1999) 2589–2603.
[62] H.T. Chung, C.M. Johnston, K. Artyushkova, M. Ferrandon, D.J. Myers, P. Zelenay, Cyanamide-derived non-precious metal catalyst for oxygen reduction, Electrochem. Commun. 12 (2010) 1792–1795.
[63] W.-J. Jiang, L. Gu, L. Li, Y. Zhang, X. Zhang, L.-J. Zhang, J.-Q. Wang, J.-S. Hu, Z. Wei, L.-J. Wan, Understanding the high activity of fe-N-C electrocatalysts in oxygen reduction: Fe/Fe3C nanoparticles boost the activity of Fe–N_x, J. Am. Chem. Soc. 138 (2016) 3570–3578.
[64] R. Cao, R. Thapa, H. Kim, X. Xu, M. Gyu Kim, Q. Li, N. Park, M. Liu, J. Cho, Promotion of oxygen reduction by a bio-inspired tethered iron phthalocyanine carbon nanotube-based catalyst, Nat. Commun. 4 (2013) 2076.
[65] U.I. Kramm, M. Lefèvre, N. Larouche, D. Schmeisser, J.-P. Dodelet, Correlations between mass activity and physicochemical properties of Fe/N/C catalysts for the ORR in PEM fuel cell via ^{57}Fe Mössbauer spectroscopy and other techniques, J. Am. Chem. Soc. 136 (2014) 978–985.